Journal of Molecular Liquids 398 (2024) 124209

Contents lists available at ScienceDirect

Journal of Molecular Liquids

journal homepage: www.elsevier.com/locate/molliq

Operando UV Resonance Raman study of DNA-ionic liquids gels

Barbara Rossi [a,b,*], Sara Catalini [c,d,e], Simone Mearini [a], Fatima Matroodi [a,d,f], Alessandro Gessini [a], Claudio Masciovecchio [a], Ines Mancini [b], Andrea Mele [g]

[a] Elettra Sincrotrone Trieste, S.S. 114 km 163.5, Basovizza, 34149 Trieste, Italy
[b] Laboratory of Bioorganic Chemistry, Department of Physics, University of Trento, Via Sommarive 14, 38123 Povo, Trento, Italy
[c] Dipartimento di Fisica e Geologia, Università di Perugia, Via Pascoli, 06123 Perugia, Italy
[d] European Laboratory for Non-Linear Spectroscopy, LENS, Via Nello Carrara 1, 50019 Sesto Fiorentino, Firenze, Italy
[e] CNR-INO, Largo Fermi 6, 50125 Firenze, Italy
[f] Department of Physics, Shahid Chamran University of Ahvaz, Ahvaz, Iran
[g] Department of Chemistry, Materials and Chemical Engineering "G. Natta", Politecnico di Milano, Piazza L. da Vinci 32, 20133 Milano, Italy

ARTICLE INFO

Keywords:
UV Resonance Raman
DNA
Ionogels
Imidazolium
Ionic liquids

ABSTRACT

Double-stranded DNA dissolved in aqueous solutions of imidazolium-based Ionic Liquids (ILs) exhibits a characteristic gel transition, leading to the formation of DNA ionogels. In this study, we utilize state-of-the-art operando UV Resonance Raman (UVRR) spectroscopy, along with UV and Circular Dichroism (CD) absorption experiments, to monitor the self-assembly of a class of DNA ionogels derived from low-concentration aqueous solutions of DNA in imidazolium-based ILs. Our experimental approach offers insights at the molecular level into the structural organization and interactions that stabilize the gel network. Furthermore, operando UVRR spectroscopy allows efficient monitoring of the different stages of the thermal pathway leading to the self-assembly of DNA/ILs solutions into ionogels. A key achievement of our study is demonstrating that the sol–gel transition in DNA ionogels in the presence of imidazolium-based ILs can be modulated by the length of the alkyl chain of the imidazolium cation to achieve desired premelting, melting, and gelation temperatures.

1. Introduction

DNA hydrogel assemblies exhibit fascinating properties for a wide variety of applications, especially in the biomedical field [1]. Biocompatibility, degradability, high versatility and capability of programmable architecture have made nucleic acids, nucleobases, nucleosides, and nucleotides unique natural building blocks for the construction of functional gel materials. For instance, DNA hydrogels have been used as an ideal platform for the controlled delivery of antigens and drugs [2–4], for tissue engineering in regenerative medicine [5] and to manufacture biosensors [6,7]. Natural and derivatized nucleobases and nucleosides can be opportunely used as gelators able to self-assemble into ordered and stable supramolecular gel structures [8]. For instance, it has been demonstrated that many guanine nucleosides and nucleotides can aggregate in water leading to the formation of self-assembled hydrogel structures with tailored properties for specific applications [9–12]. These higher-order supramolecular architectures based on nucleobases find interesting applications in the fields of nanotechnology, biology and environmental science [13,14].

Among the DNA-based gels, an emerging class of materials is that of the ionogels which are prepared by self-assembly of DNA and Ionic Liquids (ILs) [15,16] to form a hybrid material with very peculiar characteristics. In recent years, ionogels have attracted much attention due to their unique properties including ionic conductivity, desirable mechanical properties, and high thermal and electrochemical stability [15–18]. Compared to simple hydrogels, ionogels show anti-freezing properties at sub-zero temperatures and the capability of maintaining hydration for a longer time even under dry conditions. Therefore, ionogels offer an optimal alternative to hydrogels for specific applications in harsh conditions, such as at high and sub-zero temperatures [19]. Although various polymers can be employed with ILs to prepare ionogels, short or long nucleotide sequences are a promising building block for the rational design of multifunctional materials. DNA ionogels prepared using double-stranded DNA and imidazolium-based ILs by thermal treatment have been previously proposed by other authors [20–22]. In particular, the self-assembly of DNA gels prepared at a DNA concentration below 5 % w/v in aqueous solution of 1-ethyl-3-methylimidazolium chloride has been reported [21]. For these ionogels, it has been

* Corresponding author.
E-mail address: barbara.rossi@elettra.eu (B. Rossi).

https://doi.org/10.1016/j.molliq.2024.124209
Received 30 May 2023; Received in revised form 1 February 2024; Accepted 4 February 2024
Available online 8 February 2024

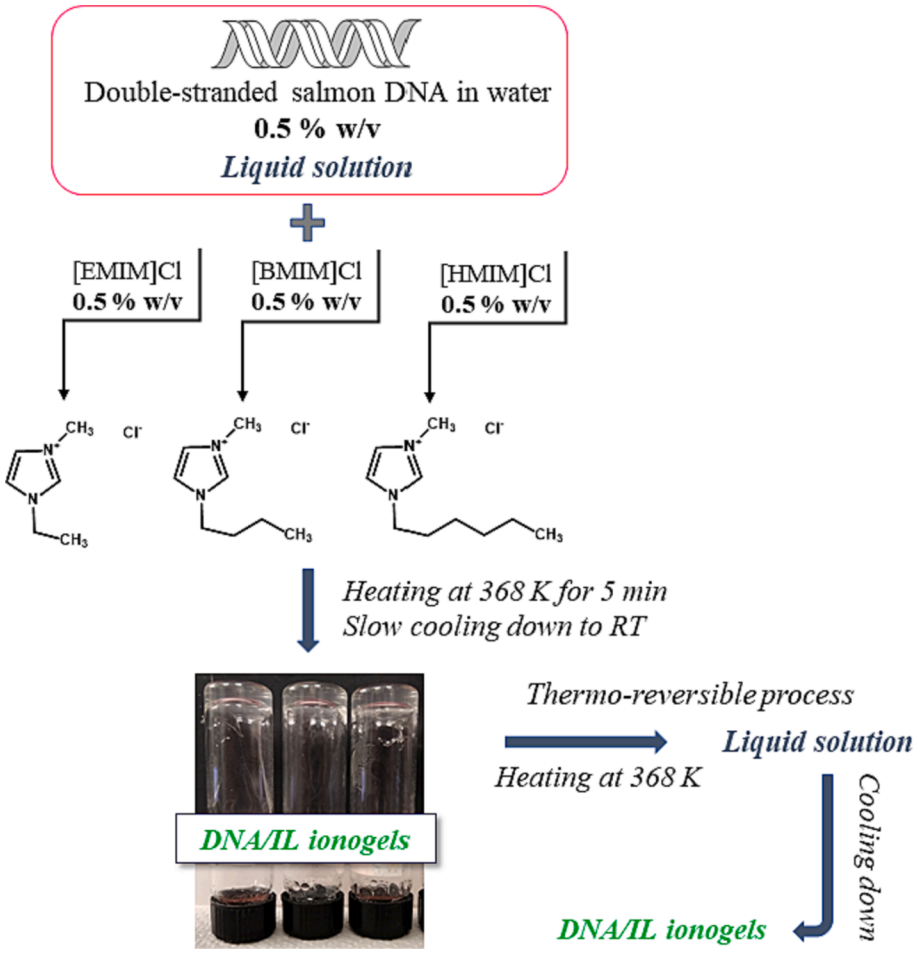

Fig. 1. Depicting of the preparation of DNA ionogels characterized in this study: the IL ([EMIM]Cl, [BMIM]Cl or [HMIM]Cl 0.5 % w/v) was added to double stranded salmon DNA dissolved in water (0.5 % w/v), the mixed solution was heated and then slowly cooled down to room temperature thus obtaining the transparent gels. The process thermo-reversibility was verified.

observed that the gelation temperature in the range of 60–67 °C can be controlled by the concentration of ionic liquid in the DNA solution. Additionally, rigid ionogels can be prepared at DNA concentration below 1 % w/v by using a longer alkyl chain imidazolium-based IL such as 1-octyl-3-methylimidazolium chloride [22]. A phenomenological explanation has been proposed for the gelation mechanism of 2000 base pairs DNA in an aqueous solution of methylimidazolium-based ILs [21,22]. As a first step, the establishment of hydrogen bonds between the nucleotides and the nitrogen groups on imidazolium cation likely prevents the re-formation of the helix structure of DNA after thermal denaturation. These H-bonds interactions contribute to keep separate the two strands of DNA. Subsequently, the self-assembly of the DNA strands occurs with the hydrophobic alkyl chains of IL cation which form the physical entanglements of the gel network [21,22]. The physical parameters of the resulting gels, such as gelation temperature and viscoelastic properties, are strongly dependent on the length of the alkyl chain on the imidazolium cation.

The selection of DNA ionogel components and the preparation method need to meet some criteria which depend on the final characteristics of the gels. In particular, the control of the key parameters during the gelation process of DNA is crucial to obtaining materials with specific properties for selected applications. To this aim, the detailed characterization of DNA ionogel structure, at a molecular level, is desirable and of great significance. However, this is challenging in some cases because of the structural complexity, the large size and the high water content of these materials.

UV Resonance Raman (UVRR) spectroscopy is a powerful method for the sensitive and selective local probing of the structure and the environment of DNA bases, even in the presence of aqueous solvents or ILs [23]. Thanks to the resonance effect, UVRR technique enables us to overcome some of the limitations of the standard visible Raman spectroscopy. By using an ultraviolet excitation wavelength where the DNA bases absorb [24,25], the Raman signals associated with the nucleobase rings are dramatically enhanced over those derived from the aqueous buffer and DNA backbone. This provides the opportunity for a selective label-free detection of vibrational markers of the hydrogen bond strength and stacking forces involving specific tracts of DNA [23,26,27]. UV Resonance Raman technique has been also successfully implemented to resolve various types of DNA structural motifs and to effectively monitor subtle changes in their local geometry and/or interactions [28–30].

Since UVRR method is not destructive and it does not require any pre-treatment or handling of the sample, this can be applied to the study of complex DNA assemblies *in situ* and *operando* conditions. The operando UVRR measurements possess inherent advantages for the characterization of DNA ionogels because they combine molecular selectivity and sensitivity with the capability to monitor the self-assembly of the gel network directly during its formation and in the hydrated state. This provides direct insights into the gelation mechanism of DNA ionogels as a function of the key parameters which can be varied in the preparation.

Here we exploit the state-of-the-art operando UVRR technique, in combination with conventional UV and Circular Dichroism (CD) absorption experiments, to provide a comprehensive description of the self-assembly mechanism of a class of thermo-reversible ionogels

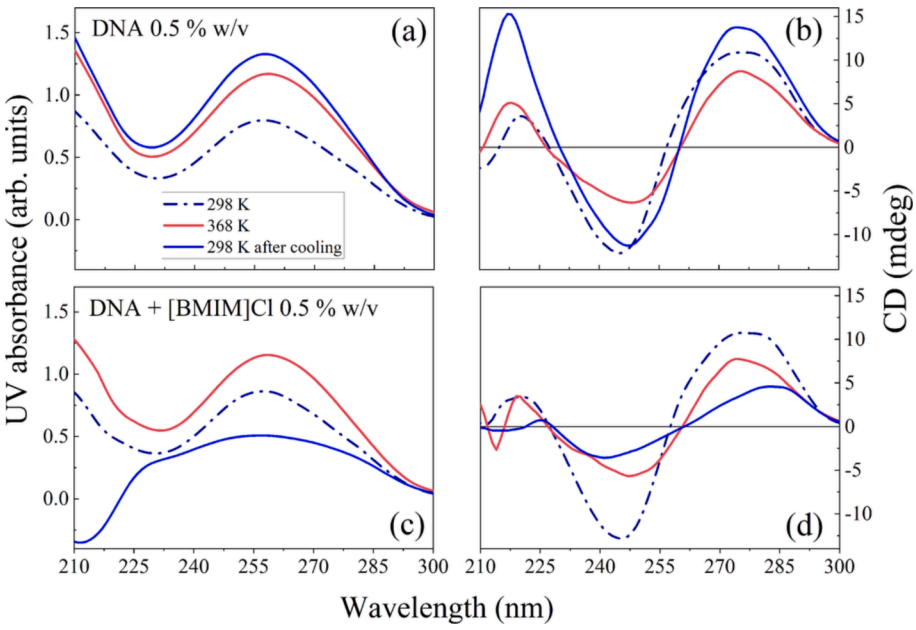

Fig. 2. Representative UV absorption and CD spectra of DNA 0.5 % w/v in water (a)-(b) and aqueous solution of DNA + [BMIM]Cl 0.5 % w/v (c)-(d) collected at 298 and 368 K, before and after cooling.

obtained by low-concentrated aqueous solutions of DNA (0.5 % w/v) in imidazolium-based ILs. In particular, we aim to explore the effect on the self-assembly and gelation behaviour of DNA as the length of the alkyl chain on the imidazolium cation varies. We expect that the lengthening of the hydrophobic tails on IL affects the clustering properties of DNA in the ionogels, in turn influencing their gelation behaviour.

2. Experimental methods

2.1. Preparation of DNA ionogels

DNA sodium salt from salmon testes (CAS number 438545–06-3, ≈2000 base-pairs, MW = 1.3 x 10^6 Da, G–C content: 41.2 %) was purchased from Sigma-Aldrich and used without further purification. The ionic liquids 1-ethyl-3-methylimidazolium chloride [EMIM]Cl, 1-butyl-3-methylimidazolium chloride [BMIM]Cl and 1-hexyl-3-methylimidazolium chloride [HMIM]Cl were acquired from IoLiTec with a purity of 99 %.

All DNA ionogel samples were prepared by adapting the protocol proposed by Pandey at al. [21,22]. The double-stranded salmon DNA and the ILs were mixed in deionized water at the same weight/volume (% w/v) concentration. The solutions were heated at 368 K for some minutes to denature DNA, followed by slow cooling to room temperature. After this treatment, the formation of strong, transparent gels is observed (see scheme of Fig. 1). A set of three different DNA ionogels was prepared by mixing DNA and [EMIM]Cl, [BMIM]Cl and [HMIM]Cl in water at the same final concentration of 0.5 % w/v. The thermoreversible formation of the ionogels was eventually verified.

All the DNA/IL solutions were freshly prepared and analysed by UVRR and CD/UV spectroscopies as a function of temperature both during the heating and the cooling cycle until the formation of the ionogels.

2.2. UVRR measurements

UV Resonance Raman spectra were collected by exploiting the multi-wavelengths UVRR set-up available at the BL10.2-IUVS beamline of Elettra Sincrotrone Trieste (Italy) [31]. The spectra were recorded using the excitation wavelength at 266 nm provided by a CryLas FQSS 266-Q2, Diode Pumped Passively Q196 Switched Solid State Laser. The vertical polarized VV Raman spectra were collected in back-scattered geometry, analysed by using a single pass of a Czerny-Turner spectrometer (Trivista 557, Princeton Instruments, 750 mm of focal length) equipped with holographic grating at 1800 g/mm and detected with a UV-optimized CCD camera. The calibration of the spectrometer was standardized using cyclohexane (spectroscopic grade, Sigma Aldrich). The final radiation power on the samples was kept at about 0.2 mW. Any possible photo-damage effect due to a prolonged exposure of the sample to UV radiation was avoided by continuously spinning the sample cell during the measurements. The comparison between the individual spectra acquired repeatedly for each sample showed no gradual changes to the spectra with respect to accumulation number, ensuring that no sample photodegradation due to UV radiation was observed. The UVRR spectra of the DNA solutions were measured in the temperature range 296–368 K both during heating and cooling using a sample holder equipped with a thermal bath coupled to a resistive heating system for controlling the temperature of the sample (stability of ± 0.1 K). Before starting with the acquisition of the UVRR spectrum, the samples were equilibrated at each temperature for 2 min.

2.3. Off-resonance Raman measurements

Out of Resonance Raman spectra were collected at room temperature by using an integrated micro-Raman setup (Horiba-JobinYvon, LabRam Aramis) with exciting radiation at 632.8 nm provided by a He-Ne laser. The resolution was set at about 0.7 cm^{-1}/pixel.

2.4. Circular dichroism and UV absorption measurements

Circular dichroism (CD) and UV absorption spectra of DNA ionogels were simultaneously recorded using a Jasco J-810 polarimeter equipped with a plug-n-play single-cell Peltier for temperature control. All the solutions of DNA and IL were freshly prepared in a demountable rectangular suprasil quartz cell of 0.1 mm path length (Hellma) and measured as a function of temperature in the range 298–368 K during the heating and the cooling cycle. A short optical path length of the cell has been opportunely selected to prevent UV absorption saturation in the 200–300 nm wavelength range due to the high concentration of DNA

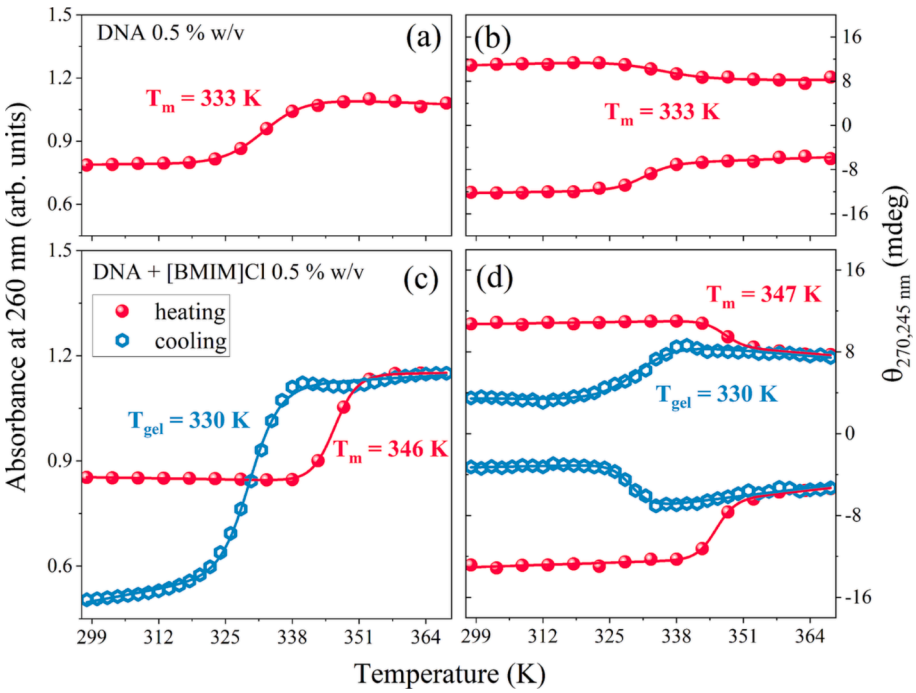

Fig. 3. Temperature-dependence of UV absorbance at 260 nm and of ellipticity θ_λ at 245 and 270 nm for DNA in water 0.5 % w/v (a)-(b) and for aqueous solution of DNA + [BMIM]Cl 0.5 % w/v (c)-(d) during heating and cooling cycle. The values of absorbance and ellipticity were extracted by the UV and CD spectra. The full lines are fitting of the experimental data as described in the experimental method section.

samples. Before starting with the acquisition of the spectra, the solutions were equilibrated at each temperature for 1 min. Each CD and UV spectrum was collected in the range from 205 to 320 nm with an increment of 1 nm, a 50 nm/min scan rate and a 1 nm bandpass. Measurements were performed under a constant nitrogen flow. For each set of temperature-dependent measurements, the spectra of the pure buffer in water and in water/IL solution were subtracted from the corresponding spectra of the samples. The exact values of the ellipticity θ_λ at 245 and 270 nm were directly extracted by the CD spectra. A simple two-state law equation was used to fit the CD and UV absorption melting curves for estimating the transition temperatures.

3. Results and discussion

3.1. Melting and gelation temperature detected by UV and CD spectroscopies

UV and CD absorption spectroscopies are the most widely used methods to monitor the conformational changes of nucleic acids in solution, such as the DNA melting transition from double stranded (ds) to single stranded (ss), self-assembly or the formation of supramolecular complexes. In particular, UV and CD spectra of DNA are informative on both the stacking interactions and the relative orientation of the nucleobases [32–36]. UV absorption and CD spectra of DNA and DNA+ [BMIM]Cl aqueous solutions are reported in Fig. 2(a)-(d) at the temperature of 298 K and 368 K, and collected during the heating and the subsequent cooling of the samples. All the spectra are shown in Fig. S1 and Fig. S2 of the Supplementary Information (SI).

The UV spectra of ds-DNA at 298 K in water and in water-IL solution show the maximum absorbance at around 260 nm (Fig. 2(a) and (c)). This absorption band is related to the π-π^* electronic transition of pyrimidine and purine bases [32,33]. The melting process from the ds-DNA to the ss-DNA affects the stacking and the base pairing leading to a change in the electronic configuration of the nucleobases. The DNA denaturation can be efficiently monitored by following the temperature dependence of the absorbance value at 260 nm [37].

The CD spectral features of the right-handed DNA (B-form) show the typical positive effect at about 270 nm and the negative effect at 245 nm (Fig. 2(b) and (d)) [38], whose intensity (i.e. the ellipticity θ_λ measured at the corresponding wavelengths) can be directly estimated by the measured CD spectra. The positive effect at 270 nm relates to the π-π base stacking, while the negative effect at 245 nm is associated with the ds-DNA helicity.

Fig. 2(a) shows that the intensity of the UV absorption at 260 nm of pristine DNA increases with the temperature during the heating of the solution. This effect is ascribed to the progressive disordering of the bases and the base unstacking that accompanies the thermal denaturation (melting) of double-stranded DNA in water [32,33]. In correspondence, CD spectra of ds-DNA show a decrement of the ellipticity at 270 nm and an increment at 245 nm as a consequence of the heating of the DNA water solution (Fig. 2(b)). This is consistent with a general weakening of the stacking interactions between neighbouring bases and a lessening in the helicity of ds-DNA occurring during the melting process [35,38], in agreement with UV absorption data. The observed shift of the crossover from 257 to 260 nm is a further CD spectral feature indicative of the denaturation of DNA promoted by the temperature increment [39]. Interestingly, the UV absorbance of DNA slightly further increases as the temperature lowers during the cooling of the sample, as shown in Fig. 2(a). This provides evidence that the cooling of DNA is not accompanied by the re-coiling of the bases into the Watson-Crick helix but disordered domains of single-strand DNA persist even at low temperatures. At the same time, we observe that the CD spectrum of DNA after cooling is significantly different compared with the spectrum of DNA collected at room temperature before the heating (Fig. 2(b)). This finding further confirms that the thermal denaturation of DNA is not reversible in these conditions and unusual secondary structures of ds- and ss-DNA are likely formed after thermal treatment [39].

Fig. 2(c) and (d) point out a clearly distinct behaviour of the UV absorption and CD spectral features of the aqueous solution of DNA + [BMIM]Cl during the heating and cooling cycle.

Indeed, the formation of a transparent hydrogel occurs exclusively in the solution containing [BMIM]Cl and DNA after the heating and

Table 1
Values of melting T_m and gelation T_{gel} temperatures estimated by UV and CD spectroscopies for different DNA and DNA/ILs aqueous solutions.

sample	T_m (K)	T_{gel} (K)
DNA 0.025 % w/v in water	303 ± 1	–
DNA 0.5 % w/v in water	333 ± 1	–
DNA 1 % w/v in water	337 ± 1	–
DNA + [BMIM]Cl 0.5 % w/v	346 ± 1	330 ± 1
DNA + [EMIM]Cl 0.5 % w/v	345 ± 1	328 ± 1
DNA + [HMIM]Cl 0.5 % w/v	340 ± 1	345 ± 1
DNA + [BMIM]Cl 1 % w/v	355 ± 1	327 ± 1
DNA + [EMIM]Cl 1 % w/v	357 ± 1	324 ± 1
DNA + [HMIM]Cl 1 % w/v	344 ± 1	338 ± 1

subsequent cooling process.

In correspondence with this, we observe a significant hypochromism and broadening of the UV absorption band of DNA (Fig. 2(c)). This phenomenon aligns with an increasing fraction of DNA bases stacking parallelly as the temperature decreases [32].

Similarly, both the shape and magnitude of both positive and negative effects in the CD profile of DNA above 230 nm undergo substantial changes after cooling in the presence of the ionic liquid (IL) (Fig. 2(d) and Fig S2 in SI). This behaviour indicates the distortion of the helical structure of double-stranded DNA (ds-DNA), likely attributed to the establishment of π–π stacking interactions between the DNA and the imidazolium cations of the IL.

Fig. 3(a) clearly shows that the temperature-dependent UV absorbance of DNA in water during heating follows a well-defined two-state (cooperative) trend.

The experimental points can be fitted using a sigmoidal law to estimate the characteristic melting temperature T_m = 333 K at which the transition from ds-DNA to ss-DNA occurs. A summary of the fitting outputs is reported in Table 1.

As expected, the DNA melting temperature is concentration-dependent. For the ds-DNA at 1 % w/v in water, T_m increases to 337 K, whereas in the diluted solution of DNA (0.025 % w/v), the melting point decreases to 303 K (Table 1). The temperature dependence of the ellipticity θ_λ at 245 nm and 270 nm detected for DNA 0.5 % w/v in water (Fig. 3(b)) exhibits a similar two-state melting transition in correspondence of 333 K, in line with the UV absorption data. This confirmation supports the notion that the transition from a double helix to a coil occurs without the involvement of intermediate structures.

The addition of [BMIM]Cl to water solution causes a significant increment of the DNA melting temperature from 333 K to about 346 K, as evidenced by UV absorbance and ellipticity trends reported in Fig. 3 (c)-(d). This aligns with our earlier studies, which demonstrated the ability of imidazolium-based ILs to elevate the temperature of the melting transition of ds-DNA for both short and long DNA sequences [26,27]. The reduction in both the UV absorbance and the Cotton effect during the cooling of the DNA + [BMIM]Cl solution (Fig. 3(c)-(d), blue hexagons and interpolation line) follows a cooperative law. We can associate these spectroscopic trends to the supramolecular aggregation process between DNA and the IL's components leading to the transition from a solution to a gel phase. The estimated temperature at which this gelation occurs corresponds to T_{gel} = 330 K. This is consistent with the qualitative observation of the transition of DNA/IL solution to the gel-arrested phase occuring in correspondence of about this temperature during the cooling cycle. The transition detected around 330 K during the cooling of the solution suggests the establishment of cation-mediated cross-links among DNA domains [21,22] which likely perturb the topology of the DNA structure. Based on these spectroscopic data, we can assert that the gel network of the DNA ionogel is probably stabilized by i) electrostatic forces and ii) π-π stacking interactions between single-stranded filaments of DNA, mediated by the [BMIM] cations of ILs [32].

The melting and gelation temperatures, detected by UV and CD spectroscopies, seem to be sensitive to two parameters: i) the length of the alkyl chain on the imidazolium cation of the IL, and ii) the DNA concentration (see values of T_m and T_{gel} reported in the Table 1). For instance, if the concentration of DNA is increased from 0.5 to 1 % w/v in the aqueous solution of DNA + [BMIM]Cl, T_m rises from 346 K to 355 K, whereas T_{gel} slightly decreases from 330 K to 327 K. The same behaviour (increment of T_m and decrement of T_{gel} as a function of DNA concentration) is observed also in the case of gels prepared using ILs with [EMIM] and [HMIM] as cations.

The length of the alkyl chain present in the imidazolium cation seems to affect significantly the gelation transition of the DNA ionogels. The DNA solutions prepared using [EMIM]Cl and [BMIM]Cl exhibit similar spectral modifications in both UV and CD spectra during heating and cooling (see spectra reported in Figures S1, S2 and S3). Consistently, also the corresponding melting and gelation temperatures are found to be practically the same for DNA + [BMIM]Cl and DNA + [EMIM]Cl both 0.5 % and 1 % w/v (Table 1). In contrast, the UV and CD spectra of DNA + [HMIM]Cl exhibit a behaviour more akin to those of DNA in pure water during the cooling step (see comparison between Fig. S1, S2 and S3).

This can be explained by the increased capacity of the apolar hexyl chains in the [HMIM] cation to form hydrophobic domains compared to the shorter alkyl chains of the [EMIM] and [BMIM] cations. Such an aggregation process may hamper, to some extent, the establishment of interactions between the [HMIM] cation and DNA, resulting in a minor elevation of the melting temperature of DNA in the presence of [HMIM]

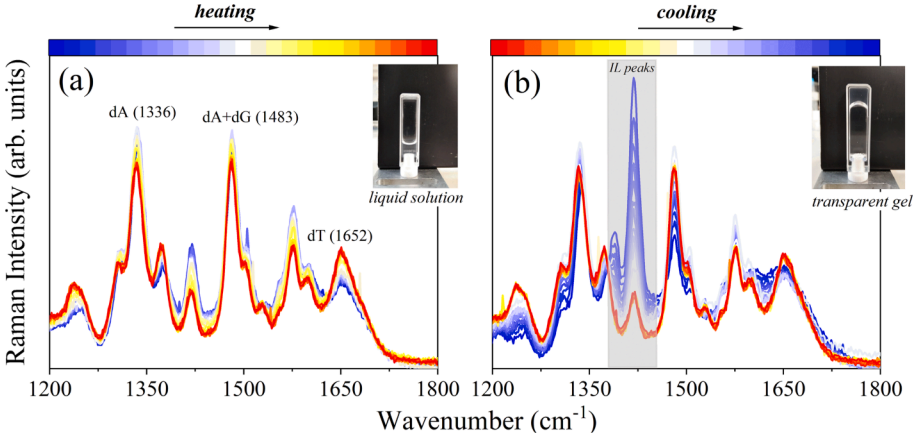

Fig. 4. 266 nm-excited UVRR spectra of the aqueous solution of DNA+[BMIM]Cl 0.5 % w/v collected between 296 and 368 K during the heating (a) and the cooling (b) cycle. The main Raman bands attributed to the DNA nucleobases are labelled in the spectra of panel (a). The Raman bands assigned to [BMIM]Cl are shadowed by grey box in the panel (b).

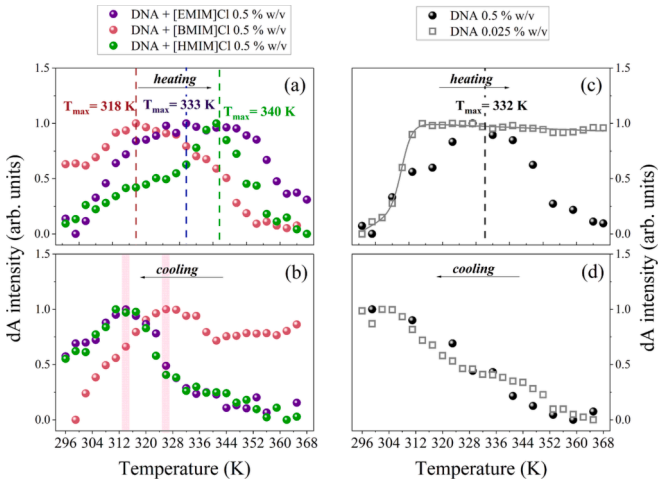

Fig. 5. Temperature dependence of the dA Raman intensity for the aqueous solutions of DNA + [BMIM]Cl 0.5 % w/v, DNA + [EMIM]Cl 0.5 % w/v and DNA + [HMIM]Cl 0.5 % w/v during heating (a) and cooling (b) cycle. The trend obtained for DNA in water at two different concentrations (0.5 % w/v and diluted solution 0.025 %w/v) during heating (c) and cooling (d) cycle is reported for comparison (full line in panel (c) is the fitting of the experimental data using a sigmoidal law). All the trends have been normalized to [0,1] for a better comparison.

Table 2
Values of T_{max} estimated from dA Raman intensity for different DNA and DNA/ILs aqueous solutions at the concentration of 0.5 % w/v.

sample	T_{max} (K)
DNA 0.5 % w/v in water	332 ± 1
DNA + [BMIM]Cl 0.5 % w/v	318 ± 1
DNA + [EMIM]Cl 0.5 % w/v	333 ± 1
DNA + [HMIM]Cl 0.5 % w/v	340 ± 1

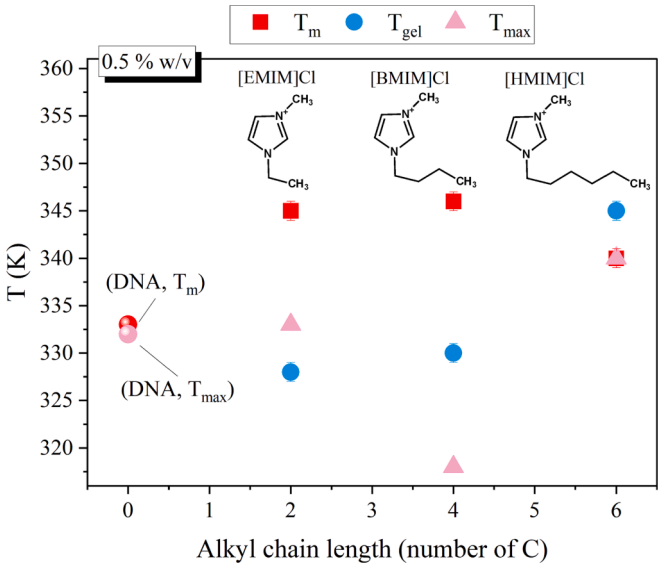

Fig. 6. Comparison between the melting T_m, gelation T_g and maximum T_{max} temperatures measured for DNA/IL aqueous solutions at concentration of 0.5 % w/v as a function of the alkyl chain length of imidazolium cation (see also Fig. 1). The values of T_m and T_{max} estimated for pristine DNA in water are also reported.

with respect to the other two IL cations. Moreover, the heightened tendency for aggregation in [HMIM]Cl may interfere with the formation of cation-DNA interactions, consistent with the higher gelation temperature (T_{gel} = 345 and 338 K for 0. 5 and 1 % w/v, respectively,) observed for DNA + [HMIM]Cl compared to the [EMIM]- and [BMIM]-based ILs (Table 1). This could be associated with the enhanced ability of the [HMIM] cation to form a network with single-stranded DNA in comparison to [EMIM] and [BMIM].

3.2. Self-organization in DNA ionogels revealed by UVRR

Fig. 4(a)-(b) present the UVRR spectra of the aqueous solution of DNA + [BMIM]Cl during the heating and cooling cycles, respectively. Using λ = 266 nm as the excitation wavelength allows us to selectively enhance the Raman bands primarily attributable to the adenine dA, guanine dG, and thymine dT nucleobases of DNA [23–25]. This enhancement is clearly evident when comparing the off-resonance spectra collected on the aqueous solutions of DNA and [BMIM]Cl at a concentration of 0.5 % w/v, and on the gel obtained by the thermal treatment of the DNA + [BMIM]Cl 0.5 % w/v solution (see Fig. S4 in the Supplementary material section). As expected, the interfering signal of water (a large bump found at about 1645 cm^{-1} and assigned to the HOH bending mode of water) dominates the visible Raman spectra of the solutions and gel in the spectral region between 1000 and 1800 cm^{-1}. Fig. S4 demonstrates that at this concentration, the characteristic spectral features of DNA are practically undetectable using an excitation wavelength far from the nucleobase resonances. Moreover, in these conditions, only the Raman peaks arising from the [BMIM]Cl can be discerned in the spectrum of the DNA + [BMIM]Cl gel sample (see Fig. S4). Conversely, the analysis of the UV resonance Raman signals of DNA in Fig. 4 provides insights into the local structural changes specifically involving these nucleobases during the formation of the ionogels.

Upon inspecting the spectra in Fig. 4(a), we can clearly identify the Raman signal dA at approximately 1336 cm^{-1}, attributed to the coupled stretching vibrations of N7 = C8 and C5-N7 bonds of the adenine ring [24,28,40–43]. This band is sensitive to any changes in stacking interactions and H-bonds at the N7 acceptor site of the adenine nucleobase. The prominent signal labeled in Fig. 4(a) as dA + dG at approximately 1483 cm^{-1} is attributed to the N7 = C8 and C8-N9 ring stretching vibrational modes coupled with C8-H in-plane deformation of purine groups in A and G bases [24,44–46]. In the 266 nm-excited spectra of DNA, this signal results from the overlapping contributions from both dA and dG residues [23]. Since both these Raman bands at approximately 1336 and 1483 cm^{-1} exhibit marked Raman intensity hypochromism upon the formation of stacked nucleic base structures [45,46], they can serve as sensitive structural markers in the investigation of DNA [23,26,27].

Finally, the band labeled as dT at approximately 1652 cm^{-1} is assigned to the stretching of C4 = O and C5 = C6 bonds of the thymine dT residues. This band can be selectively enhanced at the 266 nm excitation wavelength, allowing both signal isolation and amplification [47,48]. The substantial localization of this vibration on the C = O group of thymine makes the dT signal a sensitive marker of any perturbations occurring at this site of the thymine residues [49].

Both the UVRR spectra reported in Fig. 4(a) and (b) show remarkable changes with temperature. The signals in the region 1350–1450 cm^{-1} are attributed to the Raman modes of the ionic liquid [BMIM]Cl. They are practically negligible in the spectra of DNA/IL solution collected during the heating ramp (Fig. 4(a)) but become more and more detectable during the cooling step (see grey box in Fig. 4(b)). This is accompanied by a considerable increment in the total intensity of the characteristic OH stretching band of water (signal between 2800 and 3800 cm^{-1} not shown here) as the temperature decreases. Both these effects can be explained by the decrease in the UV absorption at 240–280 nm of the DNA/IL solution with respect to pristine DNA, as

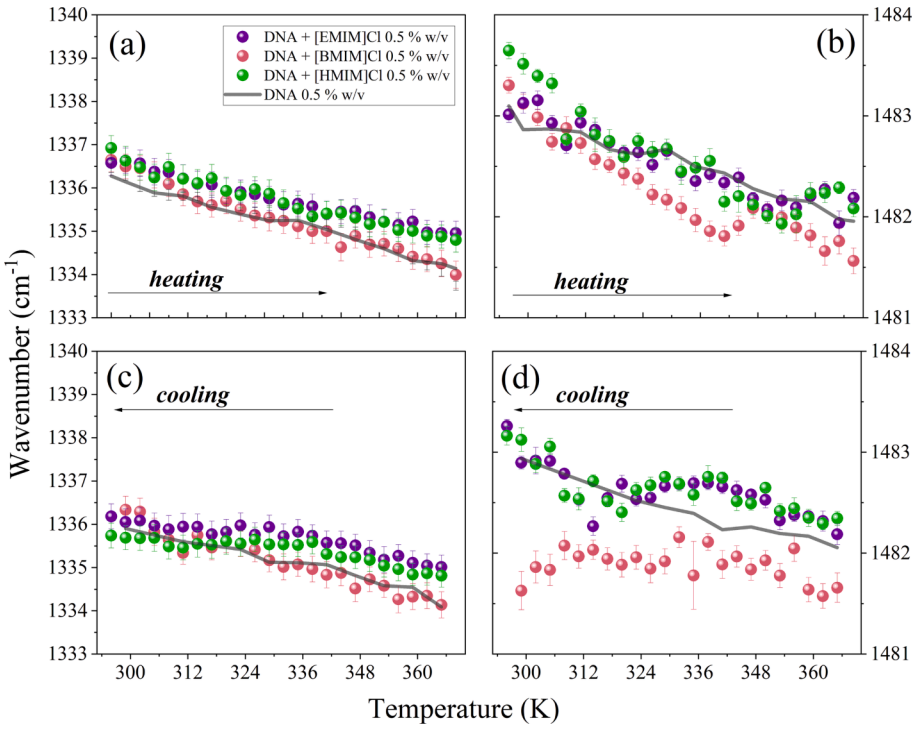

Fig. 7. Temperature dependence of the wavenumber position of dA (a)-(c) and dA + dG (b)-(d) Raman peaks for the aqueous solutions of DNA + [BMIM]Cl 0.5 % w/v, DNA + [EMIM]Cl 0.5 % w/v and DNA + [HMIM]Cl 0.5 % w/v during heating and cooling cycle. The trend obtained for pure DNA in water (0.5 % w/v) is also reported in the same panels for comparison (full line).

clearly detected in the UV absorption spectra of Fig. 2(c). Consequently, the resonant Raman cross section of the DNA peaks is reduced as well with respect to the intensity of the bands attributable to the solvent (water and IL), which become more detectable during the cooling step in Fig. 4(b). The evolution of the UVRR spectra in Fig. 4 confirms the non-reversibility of the thermal transitions of double-stranded DNA in the presence of IL. Moreover, the observed changes in the spectral parameters (intensity and frequency position) of the Raman bands of DNA can be correlated with the different solvent environment and with the DNA-IL interactions occurring during the gelation process.

3.3. Aggregation and self-assembly in DNA ionogels

Fig. 5(a)-(d) compare the temperature dependence of the intensity of the dA Raman signal at ∽1336 cm^{-1} for the three different aqueous solutions of DNA and IL examined in this study. The thermal behaviour of pure DNA in water during the heating and cooling cycles is reported in the same figure. All the trends presented in Fig. 5 have been arbitrarily normalized to [0,1] for better comparison.

As demonstrated in previous studies [23,26,27], the intensity of the Raman band dA at ∽1336 cm^{-1} serves as a reliable marker of the adenine nucleoside conformation [41]. An increase in the intensity of the dA Raman band can be attributed to two possible local effects on the adenine nucleobases: i) the partial unstacking of dA bases preceding the separation of the DNA strands during the melting transition, and/or ii) structural changes such as the enhancement of base mobility and the reversible rupture or weakening of inter-base H-bonds, which perturb but do not destroy the adenine stacking interactions [50,51].

In Fig. 5(c), the behaviour of the diluted DNA water solution during the heating step (grey squares of panel c) is consistent with the sigmoidal pattern expected for a two-state process or cooperative transition. Conversely, the points in Fig. 5(a)-(b) and the filled black points in Fig. 5 (c) do not adhere to the sigmoidal pattern of the cooperative transition. The presence of a maximum intensity vs. T recalls the localized, thermally activated structural changes (non-cooperative) related to a change in the inter-base interactions [26,27]. These processes, sometimes referred to as pre-melting and occurring at T < melting temperature T_m, likely perturb the conformations of the duplex phosphodiester backbone of DNA, but with neither significant unstacking nor dissociation of the double helix.

The fitting of the dA Raman intensity for the DNA diluted solution (full line among the empty squares in Fig. 5(c)) gives the characteristic transition temperature T_m ∽ 308 K, in good agreement with the melting temperature T_m = 303 K derived from CD and UV measurements (see Table 1). Moreover, the cooperative behaviour of dA Raman intensity for diluted DNA is consistent with our previous results obtained on similar concentrations of salmon DNA in aqueous Tris and PBS buffers at pH 7.4 [23,26].

As remarked above, the dA Raman intensity of the 0.5 % w/v DNA solution (black filled points) does not fit the two-state model but shows a well-defined maximum intensity at T_{max} = 332 K. In this case, the dA Raman signal is informative on local structural fluctuations specifically ascribed to the opening and closing of the DNA structure at the level of the adenine–thymine pairs [52]. In particular, the remarkable decrease in the dA Raman intensity observed for T > T_{max} can be related to the loss of structuration of the DNA strands as a consequence of the thermally activated base-pairs disruption. In the concentrated DNA water solution in Fig. 5(c) (black filled points), the measured T_{max} = 332 K is very close to the melting temperature T_m = 333 K (Table 1). This finding suggests that, at this DNA concentration, the thermally activated base-pair uncoupling requires the involvement of partially melted regions of DNA.

Adding the ILs to the DNA solution affects the T_{max} values, as depicted in Fig. 5(a). A summary of the observed threshold for thermal activation of the bases destructuration (T_{max}) is shown in Table 2 for DNA and DNA/IL solutions at 0.5 % w/v concentration (the values obtained for solutions at a concentration of 1 % w/v are reported in Table S1 in the SI).

The T_{max} values indicate clearly that the [BMIM] cation provides the lowest thermal threshold for base destructuration, followed by [EMIM]

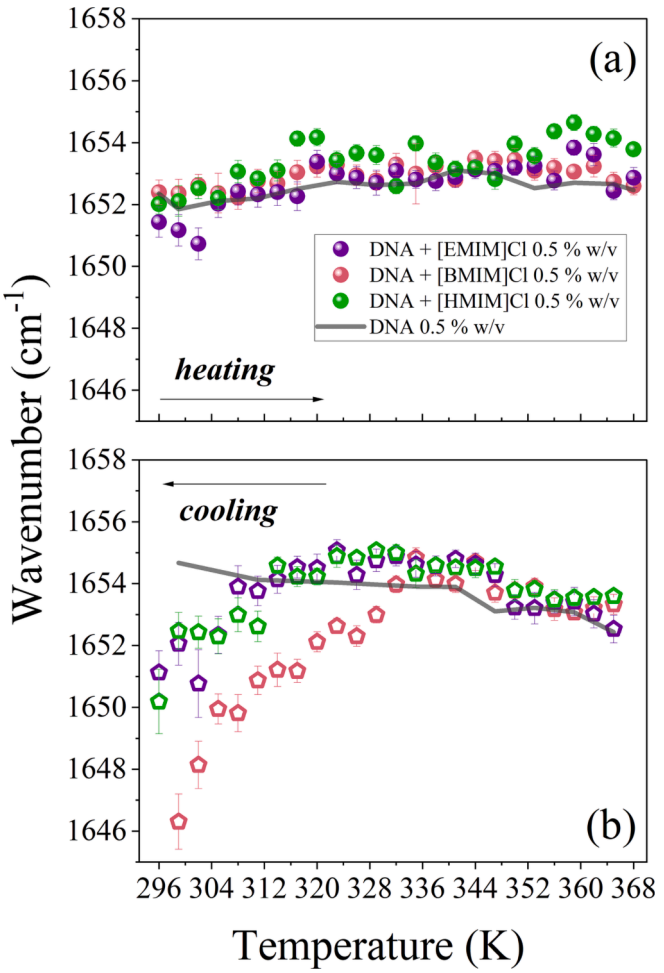

Fig. 8. Temperature dependence of the wavenumber position of dT Raman band for aqueous solutions of DNA+[BMIM]Cl 0.5 % w/v, DNA+[EMIM]Cl 0.5 % w/v and DNA+[HMIM]Cl 0.5 % w/v during heating (a) and cooling (b) cycle. The trend obtained for DNA in water (0.5 % w/v) is also reported in the same panels for comparison (full line).

and [HMIM], in that order. Although the [HMIM] doped DNA solution shows both the highest T_{max} and T_{gel} (see comparison between Table 1 and Table 2), a simple and clear-cut correlation between T_{max} and the structure of the three cations is not obvious.

Fig. 5(b) and (d) display the temperature evolution of dA Raman intensity for DNA with and without ILs during the cooling cycle. For pure DNA, both in concentrated and diluted conditions (Fig. 5(d)), we observe a slight increment in the dA Raman band intensity as the temperature decreases. This confirms the persistence of disordered, partially melted domains of DNA, independent of the solution concentration. The re-folding of DNA into its double-stranded structure during the cooling of the sample is likely hampered by the absence of salts in the water solution, thus outlining a different environment from the case of diluted solutions of DNA in saline buffer solutions [23,26]. It is known that monovalent and divalent cations present in the buffer solution are able to stabilize the duplex formation by shielding the negatively charged DNA sequence backbone.

Fig. 5(b) shows that, during the cooling of the DNA/IL solutions, the intensity of the dA Raman band exhibits a maximum corresponding to about 327 K for DNA + [BMIM]Cl and 315 K for DNA + [EMIM]Cl and [HMIM]Cl. When the temperature decreases below these values, the reduction of the UV Raman cross section of the dA Raman band is attributable to the reinforcement of the π-π stacking interactions and establishment of inter-bases cross-links among adenine residues. These interactions likely contribute to the formation and stabilization of the network structure of the DNA ionogels. The picture emerging from UVRR data fits quite well with the model proposed by Pandey et al. [21,22] for the self-assembly of the DNA ionogels. They suggest that the refolding of DNA strands after heating is prevented by the electrostatic and hydrophobic interactions between the imidazolium cation and the alkyl groups of ILs and the nucleobases of DNA.

The analysis of the temperature dependence of the intensity for the Raman band dA + dG at ∽1483 cm^{-1} reported in the Supplementary Information section (Fig. S5) shows the same trend already observed in Fig. 5 for the Raman band dA both for pure DNA and DNA/IL solutions. This confirms the sensitivity of both the two Raman bands dA and dA + dG to the establishment of stacking and inter-bases interactions involving the adenine residues in DNA.

The comparison between the melting T_m, gelation T_g, and maximum T_{max} temperatures estimated for the different DNA/IL aqueous solutions, as a function of the alkyl chain length of the imidazolium cation, is summarized in Fig. 6.

This corresponds to a possible role of dispersive force in the aggregation of the alkyl chains to form non-polar domains that, in one case, interfere with the thermal activation of the bases unpairing, thus leading to high T_{max}, and, in the other one, provide extra stabilization of the physical network of the gel, leading to higher T_{gel}. The data reported in Fig. 6 thus suggest that the alkyl chain length on the imidazolium cation is a possible trigger for the self-assembly of DNA filaments to form ionogels. The unique behaviour observed for [BMIM] cation – showing the lowest T_{max} value with respect to the other cations – is confirmed also by the trend detected for the DNA/IL solutions at 1 % w/v of concentration (see Fig. S6 in SI).

3.4. *Preferential interactions of imidazolium cations with DNA nucleobases*

Insights into localized interactions occurring at specific sites of adenine and guanine nucleobases in the DNA structure can be provided by analyzing the temperature dependence of the wavenumber position of dA and dA + dG Raman bands. It has been observed that the frequency of the oscillators associated with these Raman signals is sensitive to the different hydrogen bonding states on the proton-acceptor N7 site of guanine and adenine residues in DNA [41–43,45,46].

Fig. 7(a) illustrates the observed red-shift of the dA band of pure DNA in water with increasing temperature. This behaviour has been associated with the progressive weakening of H-bonds at the acceptor site N7 of adenine as the temperature rises [41,43]. In the case of diluted solutions of double-stranded DNA, the red-shift of the dA band has been explained by the replacement of inter-adenine H-bonds with weaker adenine–water interactions during ds-DNA unfolding (unwinding and separation). Indeed, this process is promoted by the progressive exposure to the solvent of the dA residues of DNA during the melting [41]. Fig. 7(a) shows that the addition of IL to the DNA solution does not significantly affect the wavenumber position of the dA band in the explored temperature range. This is consistent with previous observations on large and small sequences of DNA in the presence of imidazolium-based ILs, especially in a more diluted regime [26,27].

The comparison of the top and bottom panels of Fig. 7(a) reveals that DNA and DNA/ILs solutions share a reversible response to temperature variations; they both undergo a reversible dependence on temperature during the heating and cooling cycles (Fig. 7(a), at the bottom). This finding suggests that the interaction between ILs cations and DNA likely induces reversible conformational changes of adenine residues such as base tilting rather than the rupture of hydrogen bonds.

Conversely, Fig. 7(b) highlights that the frequency position of the Raman band dA + dG at ∽ 1483 cm^{-1} clearly undergoes hysteresis during the cooling of DNA/IL solutions. This is consistent with the establishment of preferential cation-mediated interactions between the imidazolium-based ILs and the guanine residues of DNA backbone

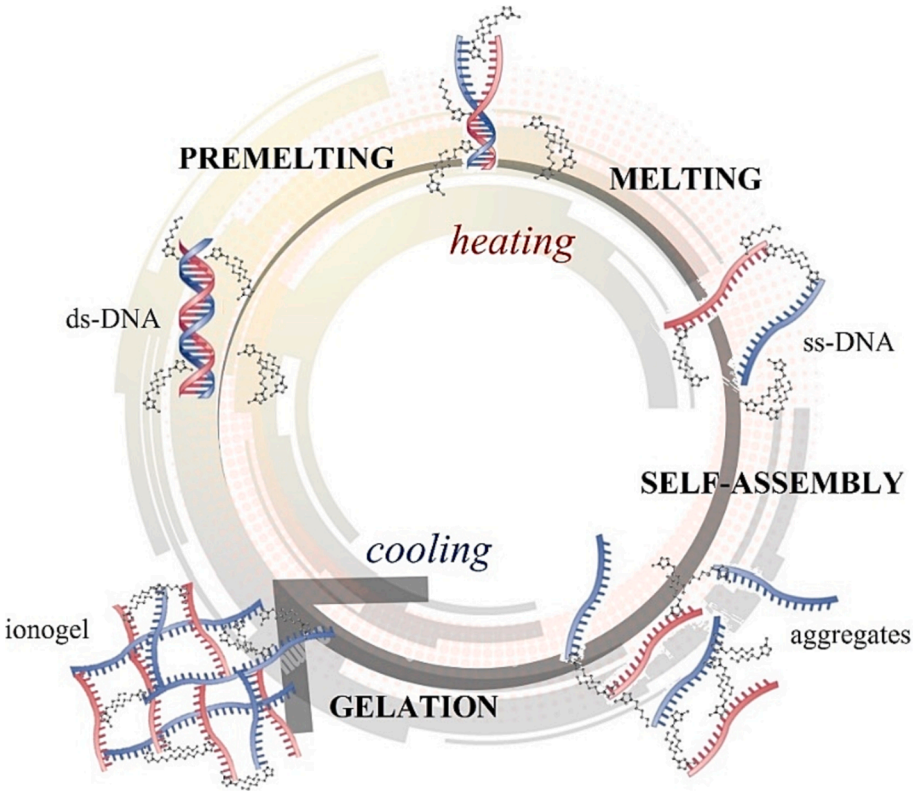

Fig. 9. Scheme of the assembly pathway leading to the formation of DNA ionogels by heating and cooling of aqueous solutions of ds-DNA and imidazolium-based ILs.

[26,27]. The observed red-shift of the dA + dG Raman band with increasing temperature, visualized in Fig. 7(b), can be explained by considering the conversion of base–base hydrogen bonds into base–solvent hydrogen bonds promoted by thermal motion during the heating ramp. During the subsequent cooling, the wavenumber position of the dA + dG Raman band does not show appreciable variations with temperature, especially in the case of the DNA + [BMIM]Cl solution. This may suggest that the network of interactions between the guanine nucleobases, mediated by the imidazolium cations, persists even during the cooling of the solution.

Finally, Fig. 8(a)-(b) illustrate the temperature dependence of the dT Raman band wavenumber position for DNA and DNA/IL aqueous solutions [24,43,49].

On heating, considering both solutions, the dT Raman band shows a very small blue-shift with increasing temperature (Fig. 8(a)). The extent of the blue-shift with increasing temperature is much less than expected based on previous results obtained on diluted solutions of DNA in buffer [23,26]. Considering the cooling step, Fig. 8(b) displays a marked red-shift of the dT Raman band position of the DNA/ILs solutions starting from about 340–330 K. This frequency shift can be correlated with the hardening of the H-bonding at the C = O site of thymine during the gelation of DNA. This interpretation is coherent with the establishment of inter-base cross-links and π-π stacking interactions as stabilizing factors of the ionogel structure during the cooling of the samples, as already detected by the trend of dA Raman intensity (Fig. 5). Finally, Fig. 8(b) shows the larger red-shift of the dT Raman band in the case of DNA + [BMIM]Cl solution, thus confirming that the [BMIM] cation is the best performing gelation agent for DNA ionogel. Overall, the trends reported in Figs. 7 and 8 seem to suggest that the structure of DNA ionogels is mainly stabilized by inter-base cross-links preferably involving the H-bonds acceptor sites of the thymine and guanine bases. These interactions are probably mediated by the imidazolium cation of ILs, in agreement with their preferential interaction with dG and dT bases in ds-DNA previously reported [26,27]. Fig. 9 summarizes the main steps of the thermal pathway leading to the formation of the DNA ionogels.

The overall transition from ds-DNA to the ionogel passes through the conversion of ds-DNA into ss-DNA. In turn, the thermally activated base-pair uncoupling of the ds-DNA occurs in two steps. In the premelting stage, the local structural fluctuations, mainly involving A-T pairs, initiate the loss of structuration of the DNA strands. This process can be efficiently monitored at the molecular level by UVRR spectroscopy. It occurs above a characteristic thermal threshold – in the present work arbitrarily indicated as T_{max} – which can be modulated by the length of the alkyl chain on the imidazolium cation. The subsequent second step is the melting of ds-DNA; it is accompanied by the base unstacking and dissociation of the double helix into ss-DNA. This phase follows a cooperative law (sigmoidal trend of the suitable physical descriptor vs T) with a characteristic transition temperature which can be precisely extracted by UV and CD absorption spectroscopy. Finally, during the cooling of the DNA/IL solutions, the self-assembly of the system and the gelation are driven by the formation of cation-mediated cross-links among DNA domains. We observe that gelation of DNA occurs through a cooperative transition at a characteristic temperature which is strongly dependent on the structure of the imidazolium cation and concentration of DNA..

4. Summary and conclusions

In this work, we investigated the microscopic structure and physical interactions in DNA ionogels obtained by the thermal treatment of an aqueous solution of double-stranded DNA and imidazolium-based ILs as a function of the alkyl chain length of the imidazolium cation.

To characterize the complex architecture of DNA ionogels and their self-organization at the molecular level, we propose a joint experimental approach combining conventional UV and CD spectroscopies with operando UV Resonance Raman scattering. Our experimental approach allows us to monitor the self-organization of DNA ionogels during the sol–gel transition, providing insights into the physical entanglements

that lead to the stabilization of the gel network. This information, complementary to that obtained from the same systems by UV and CD spectroscopies, contributes to a detailed understanding of the self-organization of DNA ionogels. Additionally, the different stages of the thermal pathway leading to the formation of the DNA ionogels can be efficiently monitored using operando UV Resonance Raman spectroscopy.

Our proposed model indicates that partially melted regions of DNA are physically cross-linked mainly through imidazolium-mediated π-π stacking interactions, which preferentially involve the guanine nucleobases of the DNA strands. UVRR data also highlight the synergistic role of alkyl chain aggregation as a stabilization factor of the gel. We demonstrate that the sol–gel transition of DNA aqueous solutions in the presence of imidazolium-based ILs can be controlled by changing the length of the alkyl chain of the imidazolium cation to obtain desired premelting, melting, and gelation temperatures. These details can facilitate the design of new synthetic strategies for the formation of DNA ionogels with improved properties.

CRediT authorship contribution statement

Barbara Rossi: Conceptualization, Data curation, Formal analysis, Investigation, Supervision, Writing – original draft, Writing – review & editing. **Sara Catalini:** Data curation, Formal analysis, Investigation, Writing – original draft, Writing – review & editing. **Simone Mearini:** Investigation. **Fatima Matroodi:** Data curation, Investigation. **Alessandro Gessini:** Software, Methodology. **Claudio Masciovecchio:** Funding acquisition, Resources. **Ines Mancini:** Investigation, Supervision, Validation, Writing – review & editing. **Andrea Mele:** Supervision, Validation, Writing – original draft, Writing – review & editing.

Declaration of competing interest

The authors declare the following financial interests/personal relationships which may be considered as potential competing interests: Barbara Rossi reports financial support was provided by Central European Research Infrastructure Consortium. Fatima Matroodi reports financial support was provided by Abdus Salam International Centre for Theoretical Physics. Sara Catalini reports financial support was provided by European Commission.

Data availability

The data that has been used is confidential.

Acknowledgments

The authors acknowledge the CERIC-ERIC Consortium for the access to experimental facilities and financial support (proposal 20192179 and 20197165). S.C. thanks the research project “FSE-REACT EU” financed by National Social Fund–National Operative Research Program and Innovation 2014-2020 (D.M. 1062/2021), personal Grant number 23-G-15445-3.

FM gratefully acknowledges funding by TRIL Program of the Abdus Salam International Centre for Theoretical Physics (ICTP).

Appendix A. Supplementary data

Supplementary data to this article can be found online at https://doi.org/10.1016/j.molliq.2024.124209.

References

[1] E. Lattuada, M. Leo, D. Caprara, L. Salvatori, A. Stoppacciaro, F. Sciortino, P. Filetici, DNA-GEL, Novel Nanomaterial for Biomedical Applications and Delivery of Bioactive Molecules, Front. Pharmacol. 11 (2020) 1345, https://doi.org/10.3389/fphar.2020.01345.

[2] M. Nishikawa, K. Ogawa, Y. Umeki, K. Mohri, Y. Kawasaki, H. Watanabe, N. Takahashi, E. Kusuki, R. Takahashi, Y. Takahashi, Y. Takakura, Injectable, self-gelling, biodegradable, and immunomodulatory DNA hydrogel for antigen delivery, J. Control. Release 180 (2014) 25–32, https://doi.org/10.1016/j.jconrel.2014.02.001.

[3] S.H. Um, J.B. Lee, N. Park, S.Y. Kwon, C.C. Umbach, D. Luo, Enzyme-catalysed assembly of DNA hydrogel, Nat. Mater. 5 (2006) 797–801, https://doi.org/10.1038/nmat1741.

[4] L. Yue, S. Wang, V. Wulf, I. Willner, Stiffness-switchable DNA-based constitutional dynamic network hydrogels for self-healing and matrix-guided controlled chemical processes, Nat. Commun. 10 (2019) 1–10, https://doi.org/10.1038/s41467-019-12697-2.

[5] E. Cheng, Y. Xing, P. Chen, Y. Yang, Y. Sun, D. Zhou, L. Xu, Q. Fan, D. Liu, A pH Triggered, Fast-Responding DNA Hydrogel, Angew. Chem. Int. Ed. 48 (2009) 7660–7663, https://doi.org/10.1002/anie.200902538.

[6] H. Yang, H. Liu, H. Kang, and W. Tan, Engineering Target-Responsive Hydrogels Based on Aptamer−Target Interactions, J. Am. Chem. Soc. 130(20) (2008) 20, 6320–6321 https://doi.org/10.1021/ja801339w.

[7] Y. Mao, J. Li, J. Yan, Y. Ma, Y. Song, T. Tian, X. Liu, Z. Zhu, L. Zhou, C. Yang, A portable visual detection method based on a target-responsive DNA hydrogel and color change of gold nanorods, Chem. Commun. 53 (2017) 6375–6378, https://doi.org/10.1039/C7CC01360D.

[8] G.M. Peters, J.T. Davis, Supramolecular gels made from nucleobase, nucleoside and nucleotide analogs, Chem. Soc. Rev. 45 (2016) 3188–3206, https://doi.org/10.1039/c6cs00183a.

[9] V. Abet, R. Rodriguez, Guanosine and isoguanosine derivatives for supramolecular devices, New J. Chem. 38 (2014) 5122–5128, https://doi.org/10.1039/c4nj00665h.

[10] T. Bhattacharyya, P. Saha, J. Dash, Guanosine-derived supramolecular hydrogels: recent developments and future opportunities, ACS Omega. 3 (2018) 2230–2241, https://doi.org/10.1021/acsomega.7b02039.

[11] J.S. Yoneda, D.R. de Araujo, F. Sella, G.R. Liguori, T.T.A. Liguori, L.F.P. Moreira, F. Spinozzi, P. Mariani, R. Itri, Self-assembled guanosine-hydrogels for drug-delivery application: Structural and mechanical characterization, methylene blue loading and controlled release, Mater. Sci. Eng. C 121 (2021) 111834, https://doi.org/10.1016/j.msec.2020.111834.

[12] F. Carducci, J.S. Yoneda, R. Itri, P. Mariani, On the structural stability of guanosine-based supramolecular hydrogels, Soft Matter 14 (2018) 2938–2948, https://doi.org/10.1039/C8SM00299A.

[13] L. Stefan, D. Monchaud, Applications of guanine quartets in nanotechnology and chemical biology, Nat. Rev. Chem. 3 (2019) 650–668, https://doi.org/10.1038/s41570-019-0132-0.

[14] T.N. Plank, L.P. Skala, J.T. Davis, Supramolecular hydrogels for environmental remediation: G(4)-quartet gels that selectively absorb anionic dyes from water, Chem. Commun. 53 (2017) 6235–6238, https://doi.org/10.1039/c7cc03118a.

[15] J. Le Bideau, L. Viaub, A. Vioux, Ionogels, ionic liquid based hybrid materials, Chem. Soc. Rev. 40 (2011) 907–925, https://doi.org/10.1039/C0CS00059K.

[16] M. Wang, J. Hu, M.D. Dickey, Tough ionogels: synthesis, toughening mechanisms, and mechanical properties-A perspective, JACS Au 2 (2022) 2645–2657, https://doi.org/10.1021/jacsau.2c00489.

[17] J. Liu, H. Song1, Z. Wang, J. Zhang, J. Zhang, X. Ba, Stretchable, self-healable, and reprocessable chemical cross-linked ionogels electrolytes based on gelatin for flexible supercapacitors, J. Mater. Sci. 55 (2020) 3991–4004, https://doi.org/10.1007/s10853-019-04271-4.

[18] C. Nan, Z. Haiqin, L. Li, C. Renjie, G. Shaojun, Ionogel Electrolytes for High-Performance Lithium Batteries: A Review, Adv. Energy Mater. 8 (12) (2018) 1702675, https://doi.org/10.1002/aenm.201702675.

[19] B. Kang, M. Gao, R. Zhao, Z. Zhao, S. Song, Multi-environmentally stable and underwater adhesive DNA ionogels enabling flexible strain sensor, Polymer 272 (2023) 125844, https://doi.org/10.1016/j.polymer.2023.125844.

[20] C.K. Lee, S.R. Shin, S.H. Lee, J.H. Jeon, I. So, T.M. Kang, S.I. Kim, J.Y. Mun, S.-S. Han, G.M. Spinks, G.G. Wallace, S.J. Kim, DNA hydrogel fiber with self-entanglement prepared by using an ionic liquid, Angew. Chem. Int. Ed. 47 (13) (2008) 2470–2474, https://doi.org/10.1002/anie.200704600.

[21] P.K. Pandey, K. Rawat, V.K. Aswal, J. Kohlbrechere, H.B. Bohidar, DNA ionogel: Structure and self-assembly, Phys. Chem. Chem. Phys. 19 (2017) 804–812, https://doi.org/10.1039/C6CP06229F.

[22] P.K. Pandey, K. Rawat, V.K. Aswal, J. Kohlbrechere, H.B. Bohidar, Imidazolium based ionic liquid induced DNA gelation at remarkably low concentration, Colloids Surf. A 538 (2018) 184–191, https://doi.org/10.1016/j.colsurfa.2017.10.083.

[23] C. Bottari, S. Catalini, P. Foggi, I. Mancini, A. Mele, D.R. Perinelli, A. Paciaroni, A. Gessini, C. Masciovecchio, B. Rossi, Base-specific pre-melting and melting transitions of DNA in presence of ionic liquids probed by synchrotron-based UV resonance Raman scattering, J. Mol. Liq. 330 (2021) 115433, https://doi.org/10.1016/j.molliq.2021.115433.

[24] S.P.A. Fodor, R.P. Rava, T.R. Hays, T.G. Spiro, Ultraviolet resonance Raman spectroscopy of the nucleotides with 266-, 240-, 218-, and 200-nm pulsed laser excitation, J. Am. Chem. Soc. 107 (6) (1985) 1520–1529, https://doi.org/10.1021/ja00292a012.

[25] S.P.A. Fodor, T.G. Spiro, Ultraviolet resonance Raman spectroscopy of DNA with 200–266-nm laser excitation, J. Am. Chem. Soc. 108 (12) (1986) 3198–3205, https://doi.org/10.1021/ja00272a006.

[26] B. Rossi, M. Tortora, S. Catalini, J. Vigna, I. Mancini, A. Gessini, C. Masciovecchio, A. Mele, A Insight into the thermal stability of DNA in hydrated ionic liquids from multi-wavelength UV resonance Raman experiments, Phys. Chem. Chem. Phys. 23 (2021) 15980–15988, https://doi.org/10.1039/D1CP01970H.

[27] F. Fadaei, M. Tortora, A. Gessini, C. Masciovecchio, S. Catalini, J. Vigna, I. Mancini, A. Mele, J. Vacek, D. Reha, B. Minofar, B. Rossi, Structural specificity of groove binding mechanism between imidazolium-based ionic liquids and DNA revealed by synchrotron-UV Resonance Raman spectroscopy and molecular dynamics simulations, J. Mol. Liq. 347 (2022) 118350, https://doi.org/10.1016/j.molliq.2021.118350.
[28] J.M. Benevides, S.A. Overman, G.J. Thomas, Raman, polarized Raman and ultraviolet resonance Raman spectroscopy of nucleic acids and their Complexes, J. Raman Spectrosc. 36 (4) (2005) 279–299, https://doi.org/10.1002/jrs.1324.
[29] F. Bianchi, L. Comez, R. Biehl, F. D'Amico, A. Gessini, A.M. Longo, C. Masciovecchio, C. Petrillo, A. Radulescu, B. Rossi, F. Sacchetti, F. Sebastiani, N. Violini, A. Paciaroni, Structure of human telomere G-quadruplex in the presence of a model drug along the thermal unfolding pathway, Nucleic Acids Res. 46 (22) (2018) 11927–11938, https://doi.org/10.1093/nar/gky1092.
[30] J. Klener, J. Štěpánek, Full UV resonance Raman analysis of temperature effects on the structural arrangement of DNA segments, J. Raman Spectrosc. 53 (3) (2021) 678–689, https://doi.org/10.1002/jrs.6057.
[31] B. Rossi, C. Bottari, S. Catalini, A. Gessini, F. D'Amico, C. Masciovecchio, Synchrotron based UV Resonant Raman scattering for material science, in V. P. Gupta, Y. Ozaki (Eds.), Molecular and Laser Spectroscopy, Elsevier: Amsterdam, The Netherlands, 2020; Chapter 13; Volume 2, pp. 447–478.
[32] I. Tinoco, Hypochromism in polynucleotides, J. Am. Chem. Soc. 82 (1960) 4785–4790, https://doi.org/10.1021/ja01503a007.
[33] W. Rhodes, Hypochromism and other spectral properties of helical polynucleotides, J. Am. Chem. Soc. 83 (1961) 3609–3617, https://doi.org/10.1021/ja01478a017.
[34] E. Brown, E.S. Pysh, Base Composition Dependence of DNA Hypochromism, J. Chem. Phys. 56 (1972) 31, https://doi.org/10.1063/1.1676865.
[35] E. Protozanova, R.B. Macgregor, Circular Dichroism of DNA Frayed Wires, Biophys. J. 75 (1998) 982–989, https://doi.org/10.1016/S0006-3495(98)77586-1.
[36] A.S. Finch, C.M. Anton, C.M. Jacob, T.J. Proctor, D.N. Stratis-Cullum, Assembly of DNA Architectures in a Non-Aqueous Solution, Nanomaterials 2 (2012) 275–285, https://doi.org/10.3390/nano2030275.
[37] G. Khandelwal, J. Bhyravabhotla, A Phenomenological Model for Predicting Melting Temperatures of DNA Sequences, PLoS One. 5 (8) (2010) e12433, https://doi.org/10.1371/journal.pone.0012433.
[38] D.S. Studdert, M. Patroni, R.C. Davis, Circular dichroism of DNA: temperature and salt dependence, Biopolymers 11 (1972) 761–779, https://doi.org/10.1002/bip.1972.360110404.
[39] D.M. Gray, R.L. Ratliff, M.R. Vaughan, Circular dichroism spectroscopy of DNA, Meth. Enzymol. 211 (1992) 389–406, https://doi.org/10.1016/0076-6879(92)11021-A.
[40] S.S. Chan, R.H. Austin, I. Mukerji, T.G. Spiro, Temperature-Dependent Ultraviolet Resonance Raman Spectroscopy of the Premelting State of dA* dT DNA, Biophys. J. 72 (4) (1997) 1512–1520, https://doi.org/10.1016/S0006-3495(97)78799-X.
[41] L. Movileanu, J.M. Benevides, G.J. Thomas Jr, Temperature Dependence of the Raman Spectrum of DNA. Part I—Raman Signatures of Premelting and Melting Transitions of Poly(dA–dT)_Poly(dA–dT), J. Raman Spectrosc. 30 (1999) 637–649, https://doi.org/10.1002/(SICI)1097-4555(199908)30:8<637::AIDJRS431>3.0.CO;2-B.
[42] N. Fujimoto, A. Toyama, H. Takeuchi, Effects of hydrogen bonding on the UV resonance Raman bands of the adenine ring and its C8-deuterated analog, J. Mol. Struct. 447 (1–2) (1998) 61–69, https://doi.org/10.1016/S0022-2860(98)00301-9.
[43] A. Toyama, H. Takeuchi, I. Harada, Ultraviolet resonance Raman spectra of adenine, uracil and thymine derivatives in several solvents. Correlation between band frequencies and hydrogen-bonding states of the nucleic acid bases, J. Mol. Struct. 242 (1991) 87–98, https://doi.org/10.1016/0022-2860(91)87129-6.
[44] Z.Q. Wen, G.J. Thomas Jr., UV resonance Raman spectroscopy of DNA and protein constituents of viruses: assignments and cross sections for excitations at 257, 244, 238, and 229 nm, Biopolymers 45 (5) (1998) 247–256, https://doiorg/10.1002/(SICI)1097-0282(199803)45:3<247::AID-BIP7>3.0.CO;2-R.
[45] J.G. Duguid, V.A. Bloomfield, J.M. Benevides, G.J. Thomas, DNA melting investigated by differential scanning calorimetry and Raman spectroscopy, Biophys. J. 71 (6) (1996) 3350–3360, https://doi.org/10.1016/S0006-3495(96)79528-0.
[46] J.G. Duguid, V.A. Bloomfield, J.M. Benevides, G.J. Thomas Jr., Raman Spectroscopy of DNA-Metal Complexes. I. The Thermal Denaturation of DNA in the Presence of Sr2+, Ba2+, Mg2+, Ca2+, Mn2+, Co2+, Ni2+, and Cd2+, Biophys. J. 69 (1995) 2623–2641, https://doi.org/10.1016/S0006-3495(95)80133-5.
[47] M. Tsuboi, M. Komatsu, J. Hoshi, E. Kawashima, T. Sekine, Y. Ishido, M.P. Russell, J.M. Benevides, G.J. Thomas, Raman and infrared spectra of (2'S)-[2'-2H] Thymidine: vibrational coupling between deoxyribosyl and thymine moieties and structural implications, J. Am. Chem. Soc. 119 (1997) 2025–2032, https://doi.org/10.1021/ja962676t.
[48] A. Jirasek, H.G. Schulze, C.H. Hughesman, A.L. Creagh, C.A. Haynes, M.W. Blades, R.F.B. Turner, Discrimination between UV radiation-induced and thermally induced spectral changes in AT-paired DNA oligomers using UV resonance Raman spectroscopy, J. Raman Spectrosc. 37 (12) (2006) 1368–1380, https://doi.org/10.1002/jrs.1552.
[49] I. Mukerji, A.P. Williams, UV resonance Raman and circular dichroism studies of a DNA duplex containing an A(3)T(3) tract: evidence for a premelting transition and three-centered H-bonds, Biochemistry 41 (2002) 69–77, https://doi.org/10.1021/bi010918i.
[50] S.C. Erfurth, W.L. Peticolas, Melting and premelting phenomenon in DNA by laser Raman scattering, Biopolymers 14 (2) (1975) 247–264, https://doi.org/10.1002/bip.1975.360140202.
[51] L. Rimai, V.M. Maher, D. Gill, I. Salmeen, J.J. McCormick, The temperature dependence of Raman intensities of DNA. Evidence for premelting changes and correlations with ultraviolet spectra, Biochim. Biophys. Acta. 361 (1974) 155–165, https://doi.org/10.1016/0005-2787(74)90343-8.
[52] A.V. Lukashin, A.V. Vologodskii, M.D. Frank-Kamenetskii, Y.L. Lyubchenko, Fluctuational opening of the double Helix as revealed by theoretical and experimental study of DNA interaction with formaldehyde, J. Mol. Biol. 108 (1976) 665–682, https://doi.org/10.1016/s0022-2836(76)80111-8.